Theor. Comput. Fluid Dyn. (2008) 22: 1–20
DOI 10.1007/s00162-007-0071-0

ORIGINAL ARTICLE

Serkan Özgen · Senem Atalayer Kırcalı

Linear stability analysis in compressible, flat-plate boundary-layers

Received: 9 January 2007 / Accepted: 20 September 2007 / Published online: 20 November 2007
© Springer-Verlag 2007

Abstract The stability problem of two-dimensional compressible flat-plate boundary layers is handled using the linear stability theory. The stability equations obtained from three-dimensional compressible Navier–Stokes equations are solved simultaneously with two-dimensional mean flow equations, using an efficient shoot-search technique for adiabatic wall condition. In the analysis, a wide range of Mach numbers extending well into the hypersonic range are considered for the mean flow, whereas both two- and three-dimensional disturbances are taken into account for the perturbation flow. All fluid properties, including the Prandtl number, are taken as temperature-dependent. The results of the analysis ascertain the presence of the second mode of instability (Mack mode), in addition to the first mode related to the Tollmien–Schlichting mode present in incompressible flows. The effect of reference temperature on stability characteristics is also studied. The results of the analysis reveal that the stability characteristics remain almost unchanged for the most unstable wave direction for Mach numbers above 4.0. The obtained results are compared with existing numerical and experimental data in the literature, yielding encouraging agreement both qualitatively and quantitatively.

Keywords Laminar boundary layers · Stability of laminar flows · Viscous instability · Inviscid instability · Compressible flows

PACS 47.15.Cb, 47.15.Fe, 47.20.Gv, 47.20.Cq, 47.40.x

1 Introduction

Laminar-turbulent transition is still an important and fundamental issue in fluid mechanics and aerodynamics. Transition location plays an important role in a number of practical applications. On the one hand, it controls important aerodynamical quantities, such as heat transfer rate and skin friction drag. These have implications on heating rates for reentry vehicles, hence on the design of proper heat shields and total drag of high-subsonic transport aircraft. On the other hand, the aerodynamic noise of commercial airplanes or detection of submarines are also functions of the flows being laminar, turbulent or transitional.

Stability and transition problems of low-speed flows have been attracting considerable interest from researchers for more than a 100 years. Meanwhile, compressibility effects have been considered by fewer

Communicated by M.Y. Hussaini.

S. Özgen (✉)
Department of Aerospace Engineering, Middle East Technical University, 06531 Ankara, Turkey
E-mail: sozgen@ae.metu.edu.tr

S. A. Kırcalı
Flight Sciences Department, Turkish Aerospace Industries, Inc., 06531 Ankara, Turkey
E-mail: satalayer@tai.com.tr

researchers due to the complexity of the resulting problem. Compressibility makes the stability and transition problems not only more complex but also more realistic for most aerodynamical problems of interest.

An early important contribution to the study of compressible flow instability was provided by Lees and Lin [1]. They have classified the disturbances as subsonic, sonic or supersonic, according to the disturbance phase velocity c_r is greater than, equal to or less than $U_\infty - a_\infty$, U_∞ and a_∞ being the freestream velocity and the freestream speed of sound, respectively. It is shown in Sect. 4 that supersonic disturbances result in a new instability mode, that is inviscid in nature. They have also proven that a necessary condition for the existence of an unstable disturbance is

$$\left[\frac{\mathrm{d}}{\mathrm{d}y}\left(\rho\frac{\mathrm{d}U}{\mathrm{d}y}\right)\right]_{y_s} = 0, \tag{1.1}$$

provided that $U(y_s) > U_\infty - a_\infty$, where ρ is the density, U the streamwise mean velocity component of the flow, y the normal distance from the wall and y_s is the location where the above equality is satisfied. This is the *generalized inflection point theorem* and is the extension of the well-known *inflection point theorem* (or *Rayleigh's theorem*) in incompressible flow.

Later, Mack developed a complete theory for the stability problem of compressible boundary layers [2,3] and has undertaken a numerical solution. According to his results, whenever there is a relative supersonic region in the flow, i.e., $\tilde{M} = (U - c_r)/a > 1$, there exists an infinite number of unstable modes (or wave numbers). The first of these modes is related to the *Tollmien–Schlichting mode* in incompressible flow, but the higher or additional modes have no incompressible counterparts. Viscosity has a stabilizing effect on the additional modes and the first of these higher modes or the second mode is the most unstable of all. After these findings, the second mode has been aptly called the *Mack mode*. In contrast to incompressible flow, where a two-dimensional disturbance is the most unstable at any Reynolds number (Squire's theorem), for supersonic flow, the most unstable disturbance is always three-dimensional, i.e., oblique [2]. Mack has obtained results using the linear stability theory (LST) followed by the e^n method for transition prediction.

Malik [4] has reported transition computations for flat-plates and sharp cones using LST and e^n method. It is shown that the first oblique Tollmien–Schlichting mode is responsible for transition for freestream Mach numbers below 7 at adiabatic conditions. For cold walls, the role of the second mode becomes dominant, and favorable pressure gradient and suction stabilize this mode.

Arnal [5] gives an extended overview of transition prediction over adiabatic flat-plates using linear theory. For two-dimensional flows, he discusses the incompressible and compressible cases independently. The basic concepts of the LST are explained and the reported results for compressible boundary layers are in agreement with those of Mack.

Masad and Abid [6] have investigated the instability of high speed, flat-plate boundary-layer flows. They have used the LST for both plane and oblique wave cases, and e^n method to predict the transition location corresponding to the most unstable wave direction. The first of higher modes and its variation with Mach number have been investigated for both adiabatic and cooled/heated flows. In the adiabatic case, the most unstable waves for the first mode are oblique, whereas those for the second mode are two-dimensional.

Another high speed boundary-layer stability analysis was performed by Malik and Anderson [7]. In their study, the effect of reacting chemistry on the instability mechanism was investigated by using perfect, chemical equilibrium and non-equilibrium (with thermal equilibrium assumption) gas models within the framework of parabolized stability equations (PSE). The results conclude that real gas effects have stabilizing effect on the first mode while they destabilize the second mode.

In a more recent publication, Malik [8] has analyzed boundary-layer transition data from supersonic quiet tunnels and flight tests. The analysis indicates that LST can be used as a guideline for transition location prediction. Transition data from the flight tests have been analyzed using PSEs, including chemistry effects associated with high temperature flows. The results indicate that transition is caused by the amplification of the second mode disturbances and the e^n method correlates the transition data well. The effect of chemistry is destabilizing.

On the experimental side, the existence of instability waves in supersonic flow was first demonstrated by Laufer and Vrebalovich [9]. Later, experiments of Kendall [10,11] on flat-plates have provided further insight to the verification of supersonic stability theory. Reference [10] is especially important, because operation of the wind tunnel was accomplished with laminar boundary layers on the walls. This increased the accuracy in the measurement of the growth of small artificial disturbances, because the large acoustic disturbances originating from the supersonic turbulent boundary layer were absent. Kendall was also able to generate skewed, i.e., oblique disturbances with respect to the freestream flow. The experiments of Kendall were performed at Mach 4.5.

Coles' [12] experiments provide transition data for flat-plates at Mach numbers between 2.0 and 4.5, whereas transition measurements of Deem and Murphy [13] are at Mach 5 and 8. For Mach numbers below 2.0, only cone data is available except the data of Kendall at Mach 1.6 [2]. Experiments of Laufer and Marte [14] which were obtained in the same experimental facility as Coles provide transition data for cones at Mach 1.3, 1.45, 1.6, 1.8 and 2.0.

In a much more recent article, Chen et al. [15] report boundary-layer transition data on a cone and a flat-plate at $M = 3.5$ obtained at the Low-Disturbance Tunnel at NASA Langley. Transition Reynolds numbers obtained in the tunnel are an order of magnitude greater than the previous results obtained in conventional noisy wind tunnels. Transition predictions obtained using LST and e^n method with $n = 10$ are in excellent agreement with transition data obtained in the experiments.

The objective of this paper is to investigate the stability issue of compressible, flat-plate boundary layers under adiabatic wall conditions. Compared to the previous studies reported in the literature, a wider range of Mach numbers is treated extending well into the hypersonic range. Real gas effects are partially accounted for both in the mean flow and the perturbation equations by taking all fluid properties including the specific heat and the Prandtl number as temperature-dependent. An extensive parametric study is performed to assess the role of relevant parameters like the Mach number and wave angle on the stability mechanism. Using known and well-proven methods, the new set of data obtained in the current study both widens the already available numerical data on the subject and provides an independent check. Also, the effect of an important parameter, the reference temperature, which is an issue that has not been elaborated sufficiently in the literature is emphasized. With these efforts, the capabilities of the LST are once more ascertained and more physical insight to the problem is provided. The study not only widens the existing data on the topic but adds new information such as the behavior of the stability characteristics when the Mach number is greater than 4.0 for oblique waves. For such high Mach numbers, the stability curves and the amplification factors become almost independent of this parameter. In our best knowledge, this result has not been reported elsewhere.

A brief outline of the paper is as follows. Section 2 of the paper is devoted to the numerical formulation of the problem. Here, the perturbation equations together with the mean flow equations are introduced. In Sect. 3, the solution method is briefly explained. Section 4 presents the results and related discussions. Here, two- and three-dimensional disturbances are treated separately. Section 5 focuses on the reference temperature issue. Comparisons with other data existing in the literature are presented in Sects. 4 and 5. Finally, in Sect. 6, important conclusions of the study are summarized.

2 Mathematical model

2.1 Stability equations

The stability equations (or the perturbation equations) are derived starting from the three dimensional equations of motion in Cartesian coordinates [16]:

$$\frac{\partial u^*}{\partial t^*} + u^*\frac{\partial u^*}{\partial x^*} + v^*\frac{\partial u^*}{\partial y^*} + w^*\frac{\partial u^*}{\partial z^*} = -\frac{1}{\rho^*}\frac{\partial p^*}{\partial x^*} + \frac{1}{\rho^*}\left(\frac{\partial \sigma^*_{xx}}{\partial x^*} + \frac{\partial \tau^*_{xy}}{\partial y^*} + \frac{\partial \tau^*_{xz}}{\partial z^*}\right), \tag{2.1}$$

$$\frac{\partial v^*}{\partial t^*} + u^*\frac{\partial v^*}{\partial x^*} + v^*\frac{\partial v^*}{\partial y^*} + w^*\frac{\partial v^*}{\partial z^*} = -\frac{1}{\rho^*}\frac{\partial p^*}{\partial y^*} + \frac{1}{\rho^*}\left(\frac{\partial \tau^*_{yx}}{\partial x^*} + \frac{\partial \sigma^*_{yy}}{\partial y^*} + \frac{\partial \tau^*_{yz}}{\partial z^*}\right), \tag{2.2}$$

$$\frac{\partial w^*}{\partial t^*} + u^*\frac{\partial w^*}{\partial x^*} + v^*\frac{\partial w^*}{\partial y^*} + w^*\frac{\partial w^*}{\partial z^*} = -\frac{1}{\rho^*}\frac{\partial p^*}{\partial z^*} + \frac{1}{\rho^*}\left(\frac{\partial \tau^*_{zx}}{\partial x^*} + \frac{\partial \tau^*_{zy}}{\partial y^*} + \frac{\partial \sigma^*_{zz}}{\partial z^*}\right), \tag{2.3}$$

$$\begin{aligned}\rho^* C^*_v\left(\frac{\partial T^*}{\partial t^*} + u^*\frac{\partial T^*}{\partial x^*} + v^*\frac{\partial T^*}{\partial y^*} + w^*\frac{\partial T^*}{\partial z^*}\right) &= -p^*\left(\frac{\partial u^*}{\partial x^*} + \frac{\partial v^*}{\partial y^*} + \frac{\partial w^*}{\partial z^*}\right)\\ &+ \frac{\partial}{\partial x^*}\left(\kappa^*\frac{\partial T^*}{\partial x^*}\right) + \frac{\partial}{\partial y^*}\left(\kappa^*\frac{\partial T^*}{\partial y^*}\right) + \frac{\partial}{\partial z^*}\left(\kappa^*\frac{\partial T^*}{\partial z^*}\right) + \mu^*\Phi^*,\end{aligned} \tag{2.4}$$

$$\frac{\partial \rho^*}{\partial t^*} + \frac{\partial(\rho^* u^*)}{\partial x^*} + \frac{\partial(\rho^* v^*)}{\partial y^*} + \frac{\partial(\rho^* w^*)}{\partial z^*} = 0, \tag{2.5}$$

$$p^* = \rho^* R^* T^*. \tag{2.6}$$

In (2.4), Φ^* is the dissipation function given by

$$\Phi^* = 2\left[\left(\frac{\partial u^*}{\partial x^*}\right)^2 + \left(\frac{\partial v^*}{\partial y^*}\right)^2 + \left(\frac{\partial w^*}{\partial z^*}\right)^2\right] - \frac{2}{3}\left(\frac{\partial u^*}{\partial x^*} + \frac{\partial v^*}{\partial y^*} + \frac{\partial w^*}{\partial z^*}\right)^2 + \left(\frac{\partial v^*}{\partial x^*} + \frac{\partial u^*}{\partial y^*}\right)^2 + \left(\frac{\partial w^*}{\partial y^*} + \frac{\partial v^*}{\partial z^*}\right)^2 + \left(\frac{\partial u^*}{\partial z^*} + \frac{\partial w^*}{\partial x^*}\right)^2. \tag{2.7}$$

In the above equations, u^*, v^* and w^* are the velocity components in x-, y- and z-directions, while p^* is the pressure, ρ^* the density and T^* the temperature. Fluid properties are represented by μ^* being the viscosity, κ^* the heat conduction coefficient, C_v^* the specific heat at constant volume and R^* the universal gas constant. While (2.1), (2.2) and (2.3) are the momentum equations in x-, y- and z-directions, respectively, (2.4) is the energy equation, (2.5) is the continuity equation and (2.6) is the equation of state. Asterisks $(*)$ denote dimensional quantities. Using Stoke's hypothesis, one obtains viscous stress components as

$$\begin{aligned} &\sigma_{xx}^* = 2\mu^* \tfrac{\partial u^*}{\partial x^*}, \quad \tau_{xy}^* = \tau_{yx}^* = \mu^*\left(\tfrac{\partial u^*}{\partial y^*} + \tfrac{\partial v^*}{\partial x^*}\right), \quad \sigma_{yy}^* = 2\mu^* \tfrac{\partial v^*}{\partial y^*}, \\ &\tau_{xz}^* = \tau_{zx}^* = \mu^*\left(\tfrac{\partial u^*}{\partial z^*} + \tfrac{\partial w^*}{\partial x^*}\right), \quad \tau_{yz}^* = \tau_{zy}^* = \mu^*\left(\tfrac{\partial v^*}{\partial z^*} + \tfrac{\partial w^*}{\partial y^*}\right), \quad \sigma_{zz}^* = 2\mu^* \tfrac{\partial w^*}{\partial z^*}. \end{aligned} \tag{2.8}$$

Flow is decomposed into steady mean and unsteady perturbations:

$$\psi^*(x^*, y^*, z^*, t^*) = \Psi^*(x^*, y^*, z^*) + \hat{\psi}^*(x^*, y^*, z^*, t^*), \tag{2.9}$$

ψ representing u^*, v^*, w^*, p^*, T^*, ρ^*, μ^* or κ^*. The following assumptions are made:

- Disturbances are small according LST, so higher order terms like $\hat{u}^* \partial \hat{u}^* / \partial x^*$ can be neglected,
- Steady mean flow satisfies the equations of motion,
- Parallel flow assumption is used, i.e., $U^* = U^*(y^*)$, $W^* = W^*(y^*)$ only and $V^* = 0$,
- Temperature is also a function of y^* only, $T^* = T^*(y^*)$,
- Fluid properties are functions of temperature only, $\mu^* = \mu^*(T^*)$, $C_v^* = C_v^*(T^*)$, $C_p^* = C_p^*(T^*)$ and $\kappa^* = \kappa^*(T^*)$.

The fluctuations of μ^* and κ^* are expressed as

$$\hat{\mu}^* = \frac{\mathrm{d}\mu^*}{\mathrm{d}T^*}\hat{T}^*, \quad \hat{\kappa}^* = \frac{\mathrm{d}\kappa^*}{\mathrm{d}T^*}\hat{T}^*. \tag{2.10}$$

With these, a linear set of equations in terms of the perturbation quantities is obtained. These equations are made dimensionless by a suitable choice of reference variables. Velocities are non-dimensionalized by U_e^* (the boundary-layer edge velocity) and lengths by the Blasius length scale $L^* = \sqrt{\nu_e^* x^* / U_e^*}$. Accordingly, the dimensionless wave number components are defined as: $\alpha = \alpha^* L^*$ and $\beta = \beta^* L^*$. Meanwhile, temperature, density, pressure, viscosity and heat conduction coefficient are non-dimensionalized by their respective free-stream values, T_e^*, ρ_e^*, p_e^*, μ_e^* and κ_e^*. The mean laminar flow is assumed to be influenced by a disturbance composed of a number of discrete harmonics, each of which is a propagating (traveling) wave of the form:

$$\hat{\psi}(x, y, z, t) = \bar{\psi}(y) e^{i(\alpha x + \beta z - \omega t)}. \tag{2.11}$$

According to temporal amplification theory, wave numbers in x- and z-directions (α and β) are real and the frequency ω is complex. The wave numbers in x- and z-directions define the wave number vector, $\mathbf{k}$. The magnitude of the wave number vector is $k = \sqrt{\alpha^2 + \beta^2}$ and the wave angle is $\Psi = \tan^{-1}(\beta/\alpha)$. The disturbance amplitude of the relevant variable is defined by $\bar{\psi}$. The real part of the complex frequency ω_r, is the circular frequency of the disturbance, while the imaginary part is the amplification rate determining whether a disturbance is stable ($\omega_i < 0$), neutrally stable ($\omega_i = 0$) or unstable ($\omega_i > 0$). Complex wave velocity is

defined as $c = \omega/\alpha$, the real part being the phase velocity c_r, and the imaginary part the amplification factor, c_i. Thus, a linear, dimensionless set of equations for the perturbations is obtained:

$$\begin{aligned}\rho\left[i\left(\alpha U+\beta W-\omega\right)\bar{u}+U^{'}\bar{v}\right] &= -i\frac{\alpha}{\gamma M^2}\bar{p}\\ &+\frac{\mu}{Re}\left\{\bar{u}^{''}-\left(\alpha^2+\beta^2\right)\bar{u}+\frac{1}{3}\left[i\alpha\bar{v}^{'}-\alpha\left(\alpha\bar{u}+\beta\bar{w}\right)\right]\right\}\\ &+\frac{1}{Re}\left\{\frac{\mathrm{d}\mu}{\mathrm{d}T}\left[T^{'}\left(\bar{u}^{'}+i\alpha\bar{v}\right)+U^{'}\bar{T}^{'}+U^{''}\bar{T}\right]+\frac{\mathrm{d}^2\mu}{\mathrm{d}T^2}U^{'}T^{'}\bar{T}\right\}, \qquad (2.12)\end{aligned}$$

$$\begin{aligned}\rho i\left(\alpha U+\beta W-\omega\right)\bar{v} &= -\frac{1}{\gamma M^2}\bar{p}^{'}+\frac{\mu}{Re}\left\{\bar{v}^{''}-\left(\alpha^2+\beta^2\right)\bar{v}+\frac{1}{3}\left[i\left(\alpha\bar{u}^{'}+\beta\bar{w}^{'}\right)+\bar{v}^{''}\right]\right\}\\ &+\frac{1}{Re}\frac{\mathrm{d}\mu}{\mathrm{d}T}\left[\left(\alpha U^{'}+\beta W^{'}\right)i\bar{T}-\frac{2}{3}T^{'}\left(i\alpha\bar{u}+i\beta\bar{w}-2\bar{v}^{'}\right)\right], \qquad (2.13)\end{aligned}$$

$$\begin{aligned}\rho\left[i\left(\alpha U+\beta W-\omega\right)\bar{w}+W^{'}\bar{v}\right] &= -i\frac{\beta}{\gamma M^2}\bar{p}\\ &+\frac{\mu}{Re}\left\{\bar{w}^{''}-\left(\alpha^2+\beta^2\right)\bar{w}+\frac{1}{3}\left[i\beta\bar{v}^{'}-\beta\left(\alpha\bar{u}+\beta\bar{w}\right)\right]\right\}\\ &+\frac{1}{Re}\left\{\frac{\mathrm{d}\mu}{\mathrm{d}T}\left[T^{'}\left(\bar{w}^{'}+i\beta\bar{v}\right)+W^{'}\bar{T}^{'}+W^{''}\bar{T}\right]+\frac{\mathrm{d}^2\mu}{\mathrm{d}T^2}W^{''}T^{'}\bar{T}\right\}, \qquad (2.14)\end{aligned}$$

$$\begin{aligned}\rho\left[i\left(\alpha U+\beta W-\omega\right)\bar{T}+\bar{v}T^{'}\right] &= -\left(\gamma-1\right)\left[i\left(\alpha\bar{u}+\beta\bar{w}\right)+\bar{v}^{'}\right]\\ &+\frac{\gamma\mu}{\sigma Re}\left[\bar{T}^{''}-\left(\alpha^2+\beta^2\right)\bar{T}+\frac{1}{\kappa}\frac{\mathrm{d}\kappa}{\mathrm{d}T}\left(2T^{'}\bar{T}^{'}+T^{''}\bar{T}\right)+\frac{1}{\kappa}\frac{\mathrm{d}^2\kappa}{\mathrm{d}T^2}\left(T^{'}\right)^2\bar{T}\right]\\ &+\gamma\left(\gamma-1\right)\frac{M^2}{Re}\left[2\mu U^{'}\left(\bar{u}^{'}+i\alpha\bar{v}\right)+2\mu W^{'}\left(\bar{w}^{'}+i\beta\bar{v}\right)\right]\\ &+\gamma\left(\gamma-1\right)\frac{M^2}{Re}\left[\frac{\mathrm{d}\mu}{\mathrm{d}T}\left(U^{'2}+W^{'2}\right)\bar{T}\right], \qquad (2.15)\end{aligned}$$

$$\rho\left[i\left(\alpha\bar{u}+\beta\bar{w}\right)+\bar{v}^{'}\right]+i\left(\alpha U+\beta W-\omega\right)\bar{\rho}+\rho^{'}\bar{v}=0, \qquad (2.16)$$

$$\bar{p}=\rho\bar{T}+T\bar{\rho}. \qquad (2.17)$$

In the above equations, $Re=\rho_e^*U_e^*L^*/\mu_e^*$ is the Reynolds number, $M=U_e^*/\sqrt{\gamma R^*T_e^*}$ the freestream Mach number, $\gamma=C_p^*/C_v^*$ the ratio of the specific heats taken to be 1.4 and $\sigma=\mu^*C_p^*/\kappa^*$ the Prandtl number. Notice that the Prandtl number is a function of temperature in this formulation and primes ($'$) denote differentiation with respect to y. Equations (2.12)–(2.14) are the momentum equations, (2.15) is the energy equation, (2.16) is the continuity equation and finally (2.17) is the equation of state. The boundary conditions for the above system at the wall and at the freestream are as follows:

$$\bar{u}(0)=\bar{v}(0)=\bar{w}(0)=\bar{T}(0)=0, \qquad (2.18)$$

$$\bar{u}(y),\bar{v}(y),\bar{w}(y),\bar{T}(y)\to 0 \quad \text{as } y\to\infty. \qquad (2.19)$$

As both the equations and the boundary conditions are homogeneous, the system constitutes an eigenvalue problem. The parameters of the problem are α, β, and Re, whereas $\omega=\omega_r+i\omega_i$ is the eigenvalue. On the other hand, $\bar{u}$, $\bar{v}$, $\bar{w}$, $\bar{p}$, $\bar{T}$, $\bar{\rho}$, $\bar{u}^{'}$ and $\bar{w}^{'}$ are the components of the eigenfunction. The above system can be put in a more convenient form for a numerical solution. For this, linear combinations of (2.12) and (2.14) are more convenient. To this end, (2.12) is multiplied by α and added to (2.14) multiplied by β. The resulting equation is now the momentum equation in the direction of the wavenumber vector $\mathbf{k}$ and replaces (2.12) in the modified system. Likewise, (2.12) is multiplied by β and subtracted from (2.14) multiplied by α. This equation in return, is the momentum equation in the direction perpendicular to the wavenumber vector and

replaces (2.14). Thus, the system of equations given above can be reduced to a system of first-order equations by defining eight new variables as follows:

$$\begin{aligned} &X_1 = \alpha\bar{u} + \beta\bar{w}, \quad X_2 = \alpha\bar{u}^{'} + \beta\bar{w}^{'}, \quad X_3 = \bar{v}, \quad X_4 = \bar{p}/\gamma M^2, \\ &X_5 = \bar{T}, \quad X_6 = \bar{T}^{'}, \quad X_7 = \alpha\bar{w} - \beta\bar{u}, \quad X_8 = \alpha\bar{w}^{'} - \beta\bar{u}^{'}. \end{aligned} \tag{2.20}$$

In terms of the new variables, the system in (2.12)–(2.17) is rewritten as

$$X_1^{'} = X_2, \tag{2.21}$$

$$\begin{aligned} X_2^{'} = &\left[i\frac{Re}{\mu T}\left(\alpha U + \beta W - \omega\right) + \left(\alpha^2 + \beta^2\right) \right] X_1 - \frac{1}{\mu}\frac{d\mu}{dT} T^{'} X_2 \\ &+ \left[\frac{Re}{\mu T}\left(\alpha U^{'} + \beta W^{'}\right) - i\left(\alpha^2 + \beta^2\right)\left(\frac{1}{3}\frac{T^{'}}{T} + \frac{1}{\mu}\frac{\mathrm{d}\mu}{\mathrm{d}T} T^{'} \right) \right] X_3 \\ &+ \left(\alpha^2 + \beta^2\right)\left[i\frac{Re}{\mu} - \frac{\gamma M^2}{3}\left(\alpha U + \beta W - \omega\right) \right] X_4 - \left[\frac{1}{\mu}\frac{\mathrm{d}\mu}{\mathrm{d}T}\left(\alpha U^{'} + \beta W^{'}\right) \right] X_6, \\ &+ \left[\frac{\left(\alpha^2 + \beta^2\right)}{3}\frac{1}{T}\left(\alpha U + \beta W - \omega\right) - \frac{1}{\mu}\frac{\mathrm{d}\mu}{\mathrm{d}T}\left(\alpha U^{''} + \beta W^{''}\right) - \frac{1}{\mu}\frac{\mathrm{d}^2\mu}{\mathrm{d}T^2} T^{'}\left(\alpha U^{'} + \beta W^{'}\right) \right] X_5, \end{aligned} \tag{2.22}$$

$$X_3^{'} = -iX_1 + \frac{T^{'}}{T} X_3 - i\gamma M^2\left(\alpha U + \beta W - \omega\right) X_4 + \frac{i}{T}\left(\alpha U + \beta W - \omega\right) X_5, \tag{2.23}$$

$$\begin{aligned} CX_4^{'} = &i\left(2\mu\frac{\mathrm{d}\mu}{\mathrm{d}T} T^{'} + \frac{4}{3}\frac{T^{'}}{T} \right) X_1 - iX_2 \\ &+ \left[\frac{4}{3}\frac{T^{''}}{T} - \left(\alpha^2 + \beta^2\right) - \frac{Re}{\mu}\frac{i}{T}\left(\alpha U + \beta W - \omega\right) + \frac{4}{3}\frac{1}{\mu}\frac{\mathrm{d}\mu}{\mathrm{d}T}\frac{T^{'2}}{T} \right] X_3 \\ &- i\frac{4}{3}\gamma M^2\left\{ \frac{T^{'}}{T}\left(\alpha U + \beta W - \omega\right) + \left(\alpha U^{'} + \beta W^{'}\right) + \frac{1}{\mu}\frac{\mathrm{d}\mu}{\mathrm{d}T} T^{'}\left(\alpha U + \beta W - \omega\right) \right\} X_4 \\ &+ \left\{ i\frac{4}{3}\left[\frac{1}{T}\left(\alpha U^{'} + \beta W^{'}\right) + \frac{1}{\mu}\frac{\mathrm{d}\mu}{\mathrm{d}T}\frac{T^{'}}{T}\left(\alpha U + \beta W - \omega\right) \right] + i\frac{1}{\mu}\frac{d\mu}{dT}\left(\alpha U^{'} + \beta W^{'}\right) \right\} X_5 \\ &+ i\frac{4}{3}\frac{1}{T}\left(\alpha U + \beta W - \omega\right) X_6, \end{aligned} \tag{2.24}$$

$$C = \frac{Re}{\mu} + i\frac{4}{3}\gamma M^2\left(\alpha U + \beta W - \omega\right), \tag{2.25}$$

$$X_5^{'} = X_6, \tag{2.26}$$

$$\begin{aligned} X_6^{'} = &-2\frac{(\gamma - 1)\sigma M^2}{\alpha^2 + \beta^2}\left(\alpha U^{'} + \beta W^{'}\right) X_2 + \left[\frac{\sigma Re}{\mu}\frac{T^{'}}{T} - 2i(\gamma - 1)\sigma M^2\left(\alpha U^{'} + \beta W^{'}\right) \right] X_3 \\ &- i\frac{(\gamma - 1)\sigma ReM^2}{\mu}\left(\alpha U + \beta W - \omega\right) X_4 + \left[\left(\alpha^2 + \beta^2\right) + i\frac{\sigma Re}{\mu T}\left(\alpha U + \beta W - \omega\right) \right. \\ &\left. - \frac{1}{\kappa}\left(\frac{\mathrm{d}\kappa}{\mathrm{d}T} T^{''} + \frac{\mathrm{d}^2\kappa}{\mathrm{d}T^2} T^{'2} \right) - \frac{(\gamma - 1)\sigma M^2}{\mu}\frac{\mathrm{d}\mu}{\mathrm{d}T}\left(U^{'2} + W^{'2}\right) \right] X_5 \\ &- \frac{2}{\kappa}\frac{\mathrm{d}\kappa}{\mathrm{d}T} T^{'} X_6 - 2\frac{(\gamma - 1)\sigma M^2}{\left(\alpha^2 + \beta^2\right)}\left(\alpha W^{'} - \beta U^{'}\right) X_8, \end{aligned} \tag{2.27}$$

$$X_7^{'} = X_8, \tag{2.28}$$

$$X_8^{'} = \frac{Re}{\mu}\frac{1}{T}\left(\alpha W^{'} - \beta U^{'}\right) X_3 - \frac{1}{\mu}\left[\frac{\mathrm{d}\mu}{\mathrm{d}T}\left(\alpha W^{''} - \beta U^{''}\right) + \frac{\mathrm{d}^2\mu}{\mathrm{d}T^2}T^{'}\left(\alpha W^{'} - \beta U^{'}\right)\right] X_5$$
$$-\frac{1}{\mu}\frac{\mathrm{d}\mu}{\mathrm{d}T}\left(\alpha W^{'} - \beta U^{'}\right) X_6 + \left[i\frac{Re}{\mu}\frac{1}{T}\left(\alpha U + \beta W - \omega\right) + \left(\alpha^2 + \beta^2\right)\right] X_7 - \frac{1}{\mu}\frac{\mathrm{d}\mu}{\mathrm{d}T}T^{'} X_8. \quad (2.29)$$

Also notice that in the above equations, ρ is replaced by $1/T$, because the equation of state in dimensionless form reads $\rho T = 1$, assuming that the mean pressure is constant across the boundary layer. The boundary conditions given in (2.18) and (2.19) are rewritten in terms of the new variables:

$$X_1(0) = X_3(0) = X_5(0) = X_7(0) = 0, \quad (2.30)$$

$$X_1(y), X_3(y), X_5(y), X_7(y) \to 0 \quad \text{as } y \to \infty. \quad (2.31)$$

2.2 Mean flow equations

The stability problem of two-dimensional, compressible flat-plate boundary-layer flows are solved in this study. Therefore, appropriate equations must be solved to account for the velocity terms (U, $U^{'}$, $U^{''}$, etc.), temperature terms (T, $T^{''}$, $T^{''}$, etc.) and temperature-dependent fluid properties in the stability equations. The velocity component in z-direction and its derivatives (W, $W^{'}$, etc.) are all zero, as the mean flow is two-dimensional. For the velocity field, the momentum equation is solved:

$$2\left(\mu^{'}U^{'} + \mu U^{''}\right) + FU^{'} = 0. \quad (2.32)$$

Notice that the above equation is a modified version of the Blasius equation in incompressible flow and F is the dimensionless streamfunction defined as $F^{'} = \rho U$. As the velocity and temperature fields are coupled in compressible flow, the energy equation must be solved simultaneously with the momentum equation. The energy equation is as follows:

$$2\left(\frac{\mu}{\sigma}T^{'}\right)^{'} + FT^{'} = -2\left(\gamma - 1\right)M^2\mu\left(U^{'}\right)^2. \quad (2.33)$$

The boundary conditions are as follows:

$$y = 0,\ F = F^{'} = 0,\ T = T_w \quad \text{or } T^{'} = 0, \quad (2.34)$$

$$y \to \infty,\ F^{'} \to 1,\ T \to 1. \quad (2.35)$$

As depicted in (2.34), either constant wall temperature or adiabatic wall boundary conditions can be treated. However, in this study only adiabatic walls are considered. The fluid properties occurring in (2.32) and (2.33) are all temperature-dependent, that are computed using the following empirical formulae [7]:

$$\frac{\mu^*}{\mu_e^*} = \left(\frac{T^*}{T_e^*}\right)^{3/2}\frac{T_e^* + S_1^*}{T^* + S_1^*}, \quad (2.36)$$

$$\kappa^* = S_2^*\frac{T^{*1/2}}{1 + \left(S_3^*/T^*\right)10^{-S_4^*/T^*}}, \quad (2.37)$$

$$C_p^* = C_{p_{\mathrm{perf}}}^*\left\{1 + \left(\frac{\gamma_{\mathrm{perf}} - 1}{\gamma_{\mathrm{perf}}}\right)\left[\left(\frac{\theta^*}{T^*}\right)^2\frac{e^{\theta^*/T^*}}{\left(e^{\theta^*/T^*} - 1\right)^2}\right]\right\}. \quad (2.38)$$

The expression in (2.36) is the well-known Sutherland's viscosity law, where $S_1^* = 110\,\mathrm{K}$, $S_2^* = 2.646 \times 10^{-3}$ W/m K, $S_3^* = 245.4\,\mathrm{K}$, $S_4^* = 12\,\mathrm{K}$ and $\theta^* = 3055\,\mathrm{K}$. Meanwhile, $C_{p_{\mathrm{perf}}}^*$ and γ_{perf} are the specific heat and ratio of specific heats for a perfect fluid, taken to be 1,006 J/kg K and 1.4, respectively. In the formulation outlined above, non-dimensional forms of the fluid properties are used. The latter are obtained by using the freestream values of the corresponding properties. The reference temperature, T_e^* has an influence on the dimensionless fluid properties, hence on the results of the analysis. For this study, it is chosen as 288 K for all the cases treated.

3 Solution method

At a distance sufficiently far away from the wall (at the uniform freestream), $U = T = \mu = \kappa = 1$ and all y-derivatives are zero to a good approximation and (2.21)–(2.29) have constant coefficients. The first six of these, (2.21)–(2.27) can be written as a system of three second-order equations:

$$X_1'' = c_{11}X_1 + c_{12}X_4 + c_{13}X_5, \tag{3.1}$$

$$X_4'' = c_{21}X_1 + c_{22}X_4 + c_{23}X_5, \tag{3.2}$$

$$X_5'' = c_{31}X_1 + c_{32}X_4 + c_{33}X_5, \tag{3.3}$$

with

$$c_{11} = \left(\alpha^2 + \beta^2\right) + i\,Re\,(\alpha U_e + \beta W_e - \omega)\,, \tag{3.4}$$

$$c_{12} = i\left(\alpha^2 + \beta^2\right)\left[Re + \frac{i}{3}\gamma M^2\,(\alpha U_e + \beta W_e - \omega)\right], \tag{3.5}$$

$$c_{13} = \frac{1}{3}\left(\alpha^2 + \beta^2\right)(\alpha U_e + \beta W_e - \omega)\,, \tag{3.6}$$

$$c_{21} = 0, \tag{3.7}$$

$$c_{22} = \left(\alpha^2 + \beta^2\right) - \frac{Re}{C_e}\left[\gamma M^2 - \frac{4}{3}\sigma\,(\gamma - 1)\,M^2\right](\alpha U_e + \beta W_e - \omega)^2\,, \tag{3.8}$$

$$c_{23} = \frac{Re}{C_e}\left(1 - \frac{4}{3}\sigma\right)(\alpha U_e + \beta W_e - \omega)^2\,, \tag{3.9}$$

$$c_{31} = 0, \tag{3.10}$$

$$c_{32} = -i\,(\gamma - 1)\,M^2\sigma\,Re\,(\alpha U_e + \beta W_e - \omega)\,, \tag{3.11}$$

$$c_{33} = \left(\alpha^2 + \beta^2\right) + i\sigma\,Re\,(\alpha U_e \beta W_e - \omega)\,, \tag{3.12}$$

with C_e defined in (2.25) evaluated at the uniform freestream:

$$C_e = Re + i\frac{4}{3}\gamma M^2\,(\alpha U_e + \beta W_e - \omega)\,. \tag{3.13}$$

Note that in the current study, $U_e = 1$ and $W_e = 0$. Equations (3.1)–(3.3) permit solutions as

$$\mathbf{X}^i = \mathbf{A}^i e^{\lambda_i y} \quad i = 1, \ldots, 6. \tag{3.14}$$

Here, λ_i are the six characteristic values, $\mathbf{X}^i$ and $\mathbf{A}^i$ are the three component solution and characteristic vectors corresponding to the i'th characteristic value, respectively. Characteristic values of the above system are

$$\lambda_{1,2} = \mp\,(c_{11})^{1/2}\,, \tag{3.15}$$

$$\lambda_{3,4} = \mp\left\{0.5\,(c_{22} + c_{33}) + 0.5\left[(c_{33} - c_{22})^2 + 4c_{23}c_{32}\right]^{1/2}\right\}^{1/2}, \tag{3.16}$$

$$\lambda_{5,6} = \mp\left\{0.5\,(c_{22} + c_{33}) - 0.5\left[(c_{33} - c_{22})^2 + 4c_{23}c_{32}\right]^{1/2}\right\}^{1/2}. \tag{3.17}$$

At the uniform freestream, (2.28) and (2.29) become decoupled from the rest of the equations and can be written as

$$X_7'' = \left[i\,Re\,(\alpha U_e + \beta W_e - \omega) + \left(\alpha^2 + \beta^2\right)\right]X_7. \tag{3.18}$$

The eigenvalues corresponding to this equation are

$$\lambda_{7,8} = \lambda_{1,2} = \mp\,(c_{11})^{1/2}\,. \tag{3.19}$$

Only the characteristic values with a negative sign are relevant because of the requirement for decaying solutions at the freestream given by (2.31). Elements of the characteristic vectors corresponding to the remaining

characteristic values can easily be found by using linear algebraic methods. These have been also verified with a commercial software [17].
Elements of the characteristic vector corresponding to λ_1 are

$$a_{11} = 1, \tag{3.20}$$
$$a_{12} = 0, \tag{3.21}$$
$$a_{13} = 0. \tag{3.22}$$

Elements of the characteristic vector corresponding to λ_3 are:

$$a_{31} = \left[c_{12}\left(c_{33} - \lambda_3^2\right) - c_{13}c_{32}\right] / \left(\lambda_3^2 - c_{11}\right), \tag{3.23}$$
$$a_{32} = c_{33} - \lambda_3^2, \tag{3.24}$$
$$a_{33} = -c_{32}. \tag{3.25}$$

Elements of the characteristic vector corresponding to λ_5 are

$$a_{51} = \left[c_{12}\left(c_{33} - \lambda_5^2\right) - c_{13}c_{32}\right] / \left(\lambda_5^2 - c_{11}\right), \tag{3.26}$$
$$a_{52} = c_{33} - \lambda_5^2, \tag{3.27}$$
$$a_{53} = -c_{32}. \tag{3.28}$$

With these, the elements of the solution vector become:

$$X_1(y) = k_1 a_{11} e^{\lambda_1 y} + k_3 a_{31} e^{\lambda_3 y} + k_5 a_{51} e^{\lambda_5 y}, \tag{3.29}$$
$$X_4(y) = k_1 a_{12} e^{\lambda_1 y} + k_3 a_{32} e^{\lambda_3 y} + k_5 a_{52} e^{\lambda_5 y}, \tag{3.30}$$
$$X_5(y) = k_1 a_{13} e^{\lambda_1 y} + k_3 a_{33} e^{\lambda_3 y} + k_5 a_{53} e^{\lambda_5 y}, \tag{3.31}$$
$$X_2(y) = k_1 a_{11}\lambda_1 e^{\lambda_1 y} + k_3 a_{31}\lambda_3 e^{\lambda_3 y} + k_5 a_{51}\lambda_5 e^{\lambda_5 y}, \tag{3.32}$$
$$X_6(y) = k_1 a_{13}\lambda_1 e^{\lambda_1 y} + k_3 a_{33}\lambda_3 e^{\lambda_3 y} + k_5 a_{53}\lambda_5 e^{\lambda_5 y}, \tag{3.33}$$
$$\begin{aligned} X_3(y) = {} & k_1 \left[\frac{-i a_{11} - i\left(\alpha U_e + \beta W_e - \omega\right)\left(\gamma M^2 a_{12} - a_{13}\right)}{\lambda_1}\right] e^{\lambda_1 y} \\ & + k_3 \left[\frac{-i a_{31} - i\left(\alpha U_e + \beta W_e - \omega\right)\left(\gamma M^2 a_{32} - a_{33}\right)}{\lambda_3}\right] e^{\lambda_3 y} \\ & + k_5 \left[\frac{-i a_{51} - i\left(\alpha U_e + \beta W_e - \omega\right)\left(\gamma M^2 a_{52} - a_{53}\right)}{\lambda_5}\right] e^{\lambda_5 y}. \end{aligned} \tag{3.34}$$

On the other hand:

$$X_7(y) = k_7 e^{\lambda_7 y}, \tag{3.35}$$
$$X_8(y) = k_7 \lambda_7 e^{\lambda_7 y}. \tag{3.36}$$

In the above equations, k_1, k_3, k_5 and k_7 are constants. These solutions provide the initial conditions for the integration of (2.21)–(2.29). A fourth-order Runge–Kutta–Fehlberg method that uses variable stepsize is employed for the integration [18]. As integration proceeds from the freestream towards the wall, the linear independence of the four solutions may be lost due to round-off error. Therefore, before this happens, Gram–Schmidt orthonormalization technique has to be used [3,19]. For this study, the algorithm is applied at every $\Delta y = 0.1$ interval and no difficulties have been encountered with. In addition, the mean flow (2.32) and (2.33) are integrated simultaneously with the stability equations employing the same Runge–Kutta–Fehlberg integrator used for the integration of the stability equations.

The stability diagrams like those shown in Fig. 3 are obtained using Newton iteration in two variables. This method requires two initial points on the curve so that the iteration can proceed in the specified Reynolds number direction. These two points are calculated using a function minimization algorithm utilizing the simplex method [20]. The Newton iteration fails at the critical Reynolds number and the procedure is repeated for the remaining branch of the curve so that the two branches meet there.

4 Results of the stability analysis

4.1 Mean velocity and temperature profiles

Figure 1 represents the velocity and temperature profiles obtained numerically by solving (2.32) and (2.33) with the boundary conditions given in (2.34) and (2.35). The second derivative of velocity is also presented, because this quantity plays an important role in the stability phenomena. In order for the stability calculations to yield accurate results, it is imperative that these profiles are produced with great accuracy.

For validation, the velocity profiles obtained in this study are compared with experimental, theoretical and numerical results reported in the literature for $M = 2.4$ and $M = 5.0$, as shown in Fig. 2. Notice that the normal distance y^* is made dimensionless by the momentum thickness θ^* in Fig. 2a and by the displacement thickness δ^* in Fig. 2b. The profiles of the current study are presented for $T_e^* = 50\,\mathrm{K}$ and $T_e^* = 288\,\mathrm{K}$ in order to demonstrate the effect of reference temperature. From the figure, it can be observed that the current profiles are in very good agreement with those reported in the literature.

Having assured the accuracy of the velocity and temperature profiles, we can now move confidently to the results of the stability analysis.

4.2 Two-dimensional disturbances

Stability data are typically presented in the form of contour plots in the $(Re - \alpha)$ plane, such as Fig. 3, where each contour is a level curve of the growth rate defined by the imaginary part ω_i of the eigenvalue. The diagrams illustrate the constant amplification curves for two-dimensional disturbances ($\beta = 0$) for different Mach numbers. In each graph, the outermost curve corresponds to $c_i = 0$, the neutral stability curve. This curve separates the unstable region ($c_i > 0$) and the stable region ($c_i < 0$), that remain inside and outside the curve, respectively.

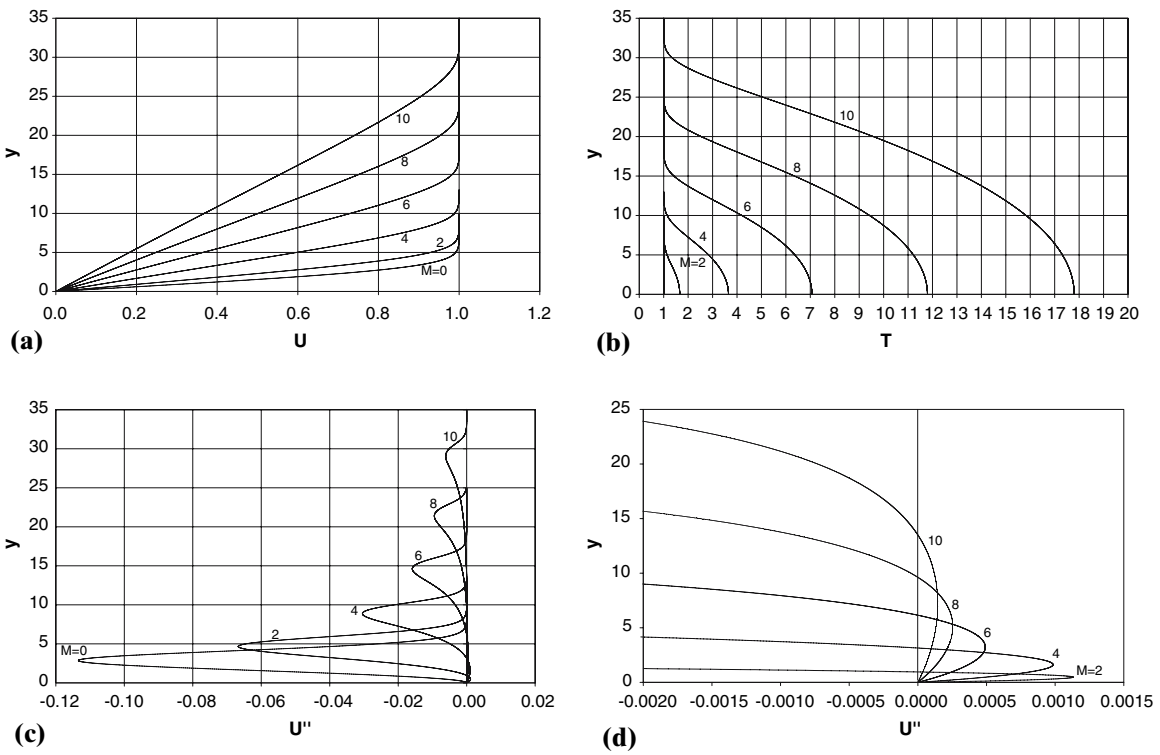


Fig. 1 Velocity and temperature profiles for compressible flat-plate boundary layers. **a** Velocity profiles, **b** temperature profiles, **c** second derivative of velocity, **d** second derivative of velocity (*expanded view*)

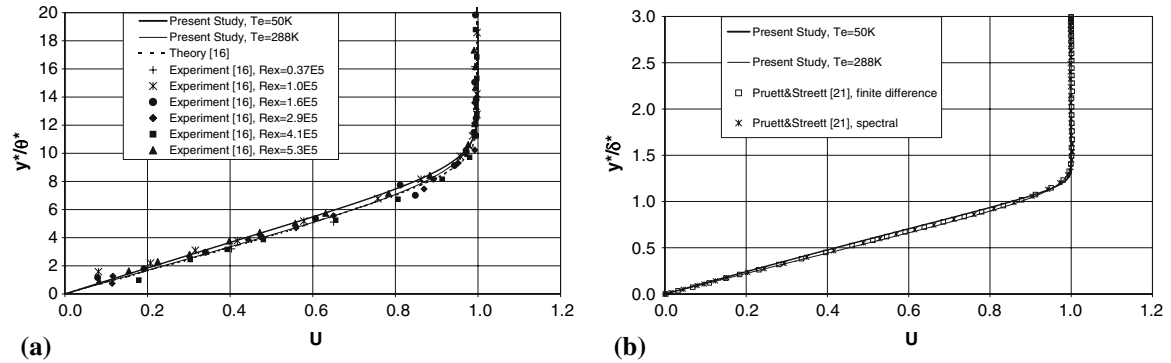


Fig. 2 Comparison of velocity and temperature profiles of the current study with theoretical, experimental and numerical profiles reported in the literature. **a** $M = 2.4$, **b** $M = 5.0$

An important outcome of the analysis is the critical Reynolds number. This is the Reynolds number, below which no amplified disturbances are observed. In other words, it is the smallest Reynolds number on the neutral stability curve. This is demonstrated on the neutral stability curve corresponding to $M = 0$.

The importance of the $M = 0$ curves is that they correspond to incompressible flow. When these curves and the corresponding critical Reynolds number are compared with those given in the literature, like Ref. [22], an excellent agreement is observed. The critical Reynolds number calculated in the present study ($R = 301.7$) agrees very well with the values given by Schlichting [16] ($R = 302.2$) and Obremski et al. [22] ($R = 302.1$).

In the interval $0 < M < 2$, although the shapes of the constant amplification factor curves do not change significantly, the amplification factors (c_i values) decrease substantially, i.e., the flow is stabilized. Viscous instability is dominant in this Mach number range, as the range of unstable wave numbers decrease as the Reynolds number increases. Obviously, compressibility has a stabilizing effect on the viscous stability mechanism in this range.

However, the stability characteristics change significantly for Mach numbers above 2. In the $M = 3$ curves for example, typical inviscid instability characteristics are observed, because the range of unstable wave numbers remain unchanged with increasing Reynolds number. For this Mach number, the amplification factors are further reduced compared to the $M = 2$ case. From these curves, we also observe that there are two isolines with the same c_i value, giving a hint for the second mode that emerges at higher Mach numbers. Indeed, $M = 4$ curves indicate that there are two distinct modes of instability. The curves at the lower part of this graph (small wavenumbers, long waves) correspond to the first mode related to the Tollmien–Schlichting mode also present in incompressible flow, whereas the curves on top (high wavenumbers, short waves) correspond to the second mode (inviscid mode or Mack mode), which has no incompressible counterpart. This mode is inviscid in nature and appears as a result of continuing reflection of acoustic waves between the wall and the relative sonic line [3]. It occurs when $\tilde{M} = (U - c_r)/a > 1$, i.e., when the disturbances are supersonic. It is also worth mentioning that at $M = 4$ the amplification factors of the first mode and the second mode have comparable magnitudes. What we also observe is that the first mode has destabilized compared to the $M = 3$ case, as the amplification factors have become higher.

When the Mach number is further increased to 6, we observe that the instability range of the second mode moves to lower wavenumbers (longer waves) accompanied by a significant destabilization judging from the magnitudes of the amplification factors. Meanwhile, the first mode instability range widens slightly, together with a noticeable increase in amplification factors.

In the $M = 7$ curves we see that the first and the second modes merge. In this case, the second mode moves down to lower wavenumbers, finally meeting the curves of the first mode. Although we now have a single neutral stability curve, the traces of two modes can still be observed, as we have two constant amplification curves for the same amplification factor, $c_i = 0.004$. There is slight destabilization compared to the $M = 6$ case but the strong destabilization trend after $M = 4$ has obviously slowed down.

The $M = 8$ curves look more like they belong to a single instability mode, but upon further examination, the legacy of the two modes is still noticeable. The unstable region has further shrunk in this case, confined to a region $0 < \alpha < 0.18$. Meanwhile, we observe no significant destabilization or stabilization compared to the $M = 7$ case, because the amplification factors are almost the same in both cases.

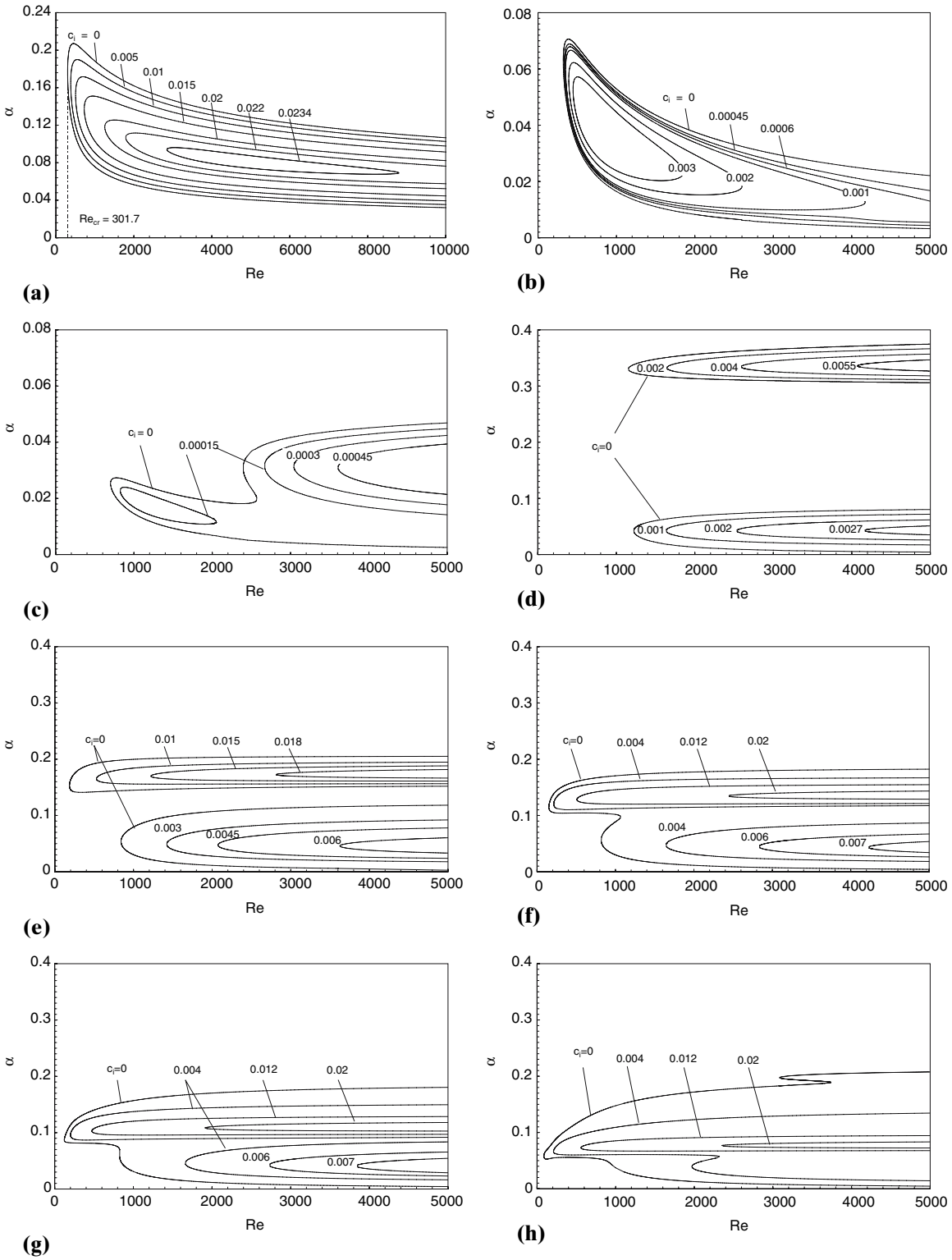


Fig. 3 Stability curves for two-dimensional disturbances. **a** $M = 0$, **b** $M = 2$, **c** $M = 3$, **d**, $M = 4$, **e** $M = 6$, **f** $M = 7$, **g** $M = 8$ and **h** $M = 10$

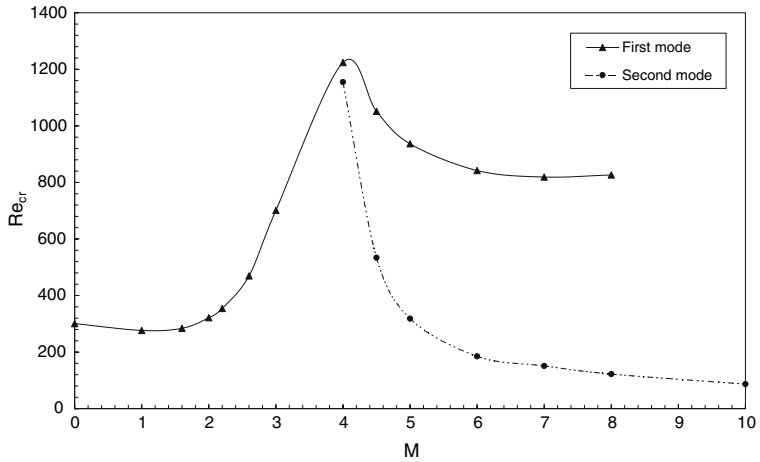


Fig. 4 Variation of the critical Reynolds number with Mach number for two-dimensional disturbances

The highest Mach number for which computations are performed is 10. The results for this Mach number are shown in the last part of Fig. 3. Here, the curves have totally merged and belong to a single mode of instability. Again, there is no significant destabilization compared to the previous case.

The summary of the stability calculations for two-dimensional disturbances is presented in Fig. 4. Here the variation of the critical Reynolds number with Mach number is illustrated. As explained above, in these computations, the second mode appears at $M = 4$ and continues to exist as a separate mode until $M = 7$. At this value of the Mach number, although there is one neutral stability curve as depicted in Fig. 3f, there are two distinct "fingers" each having its own critical Reynolds number. Both of these are included in Fig. 4. This is also the case for $M = 8$, but for $M = 10$, there is only one "finger" and only one critical Reynolds number. Therefore, only one data point exists for $M = 10$ in Fig. 4. From Fig. 3f, g, we understand that for high Mach numbers the instability is governed by the second mode. Therefore, the critical Reynolds number for $M = 10$ is included in the second mode curve, rather than the first mode curve. The two curves depicted in Fig. 4 show that the first mode is strongly stabilized between $2 < M < 4$ and is destabilized for $M > 4$. Meanwhile, the second mode is continuously destabilized with increasing Mach number. The stability characteristics of the flow treated in this study are governed by two factors. First of these is the velocity profile shape and the second is the mechanics of the instability waves. Whenever $M > 0$, due to increasing wall temperature, an inflection point in the profile occurs. If we think of the compressible flow profile as a heated wall profile to a first approximation, such profiles have destabilizing effect on the flow as demonstrated by Özgen [23]. Meanwhile, compressibility has a strong stabilizing effect on the first mode wave mechanism as inferred from the results. Among the two factors, we see that the stabilizing effect of compressibility is much more dominant in the range $2 < M < 4$ compared to the destabilizing effect of the velocity profiles.

However, this changes when $M > 4$. As the Mach number increases, the inflection point moves away from the wall as illustrated in Fig. 1, strengthening the inviscid instability mechanism. For $M > 4$, it is argued that this effect becomes more dominant compared to the stabilizing effect of compressibility, which explains the destabilization of the first mode.

As the second mode is inviscid in nature, the velocity profiles (and the corresponding inflection points) have a dominant effect on the stability characteristics for the entire range of relevant Mach numbers. This explains why we observe a continuous destabilization of this mode as the Mach number increases.

The mentioned curves are compared both qualitatively and quantitatively with the results reported by Mack [3], Arnal [5] and Masad et al. [6]. Arnal and Masad et al. have used spatial amplification formulation, while Mack has used temporal formulation similar to the current study. Mack has taken the viscosity and heat conduction coefficient as temperature-dependent but has assumed constant specific heat. The range of Mach numbers treated in his study justifies this assumption. Meanwhile, Masad et al. have taken all the fluid properties as temperature-dependent, while it is not clear how these were treated in Arnal's study. It is worth mentioning that Mack has taken the reference temperature as 50K, whereas in Masad et al.'s study it has been taken as 300K. This parameter is chosen to be 288K in the current study. Arnal has not explicitly mentioned a reference temperature, however, it can be inferred from his results that it is close to Mack's choice.

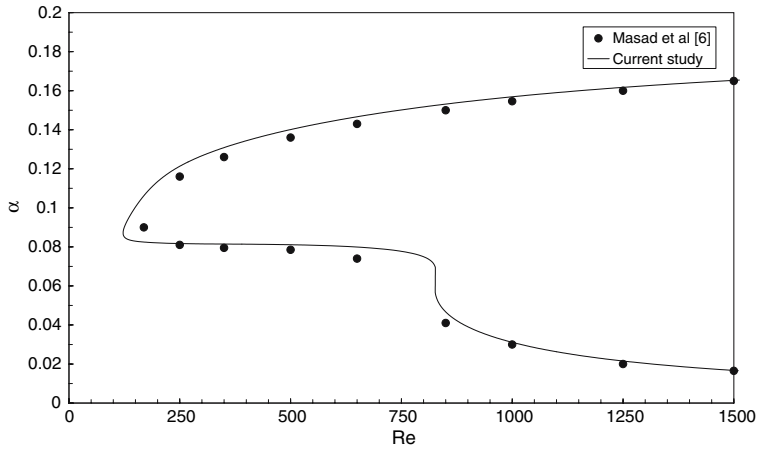


Fig. 5 Comparison of the neutral stability curve calculated in the current study with that of Masad et al. [6] for $M = 8$

The choice of the reference temperature depends on the purpose of the stability and transition calculations or the particular application. For example, on the one hand, airplanes usually fly at supersonic speeds at high altitudes where the reference temperature is low. On the other hand, missiles fly at supersonic speeds at high or low altitudes depending on the type of missile or mission, so the choice of the reference temperature depends on the application. Wind tunnel tests for supersonic flows are usually conducted at cryogenic wind tunnels where the fluid temperature is low. Therefore, if comparisons with wind tunnel data are to be made, the fluid temperature at which the wind tunnel data is obtained must be carefully determined.

Both in Mack's and Arnal's results, we observe that the effect of compressibility for $M < 2$ is small, that is in agreement with the findings of the current study. The appearance of the second mode occurs at similar Mach numbers (around 4) to the one found in the current study. Although there is disagreement in the quantities like the critical Reynolds numbers and unstable wavenumber ranges, the trends that have been outlined by Mack and Arnal are well captured by the current study. Both in Mack's and Arnal's results, the merger between the two modes occur at around $M = 4.8$, that occurs at a much higher Mach number ($M = 7$) in the current study. The shape of the neutral stability curves for higher Mach numbers are similar to those found in the current study although the numerical agreement is not very good. The disagreement can be attributed to the choice of the reference temperature for which there is a great difference between other studies and the current study, the way variable properties are represented in the mentioned studies or the different formulations used. This issue is elaborated in Sect. 5.

The agreement between the results reported by Masad et al. and the ones of the current study are much better, because the reference temperatures chosen are very close to each other, although spatial formulation is used in their study and temporal formulation in the current. It has to be noted that the empirical formulae used for the thermal conduction coefficient and the specific heat are significantly different in the two studies. There are results reported by Masad et al. that permit direct comparison. For example, their neutral stability curve for $M = 8$ is compared with the one calculated in the current study, shown in Fig. 5. As can be noted, the agreement between them is very good all around. This inference strengthens the argument that the reference temperature is a very important parameter of the problem.

4.3 Three-dimensional disturbances

The effect of wave orientation is probably best observed for $M = 4$, as both modes are present with comparable amplification factors. Figure 6 shows the effect of the wave angle on the stability characteristics of the two modes for $M = 4$. For low wave inclinations we observe that although both modes preserve their existence, there is a strong stabilization of the second mode. Moreover, for wave angles above 20° this mode ceases to be unstable. We can say this not only because the critical Reynolds numbers for this mode increase continuously with increasing wave angle, but also because of the considerable decrease in the amplification factors. Meanwhile, the first mode continuously destabilizes with increasing wave angle. The reduction in the critical Reynolds number is significant but what is more significant is the rapid increase in the amplification factors. There is, however, no significant change in the unstable wave number range for low and moderate wave

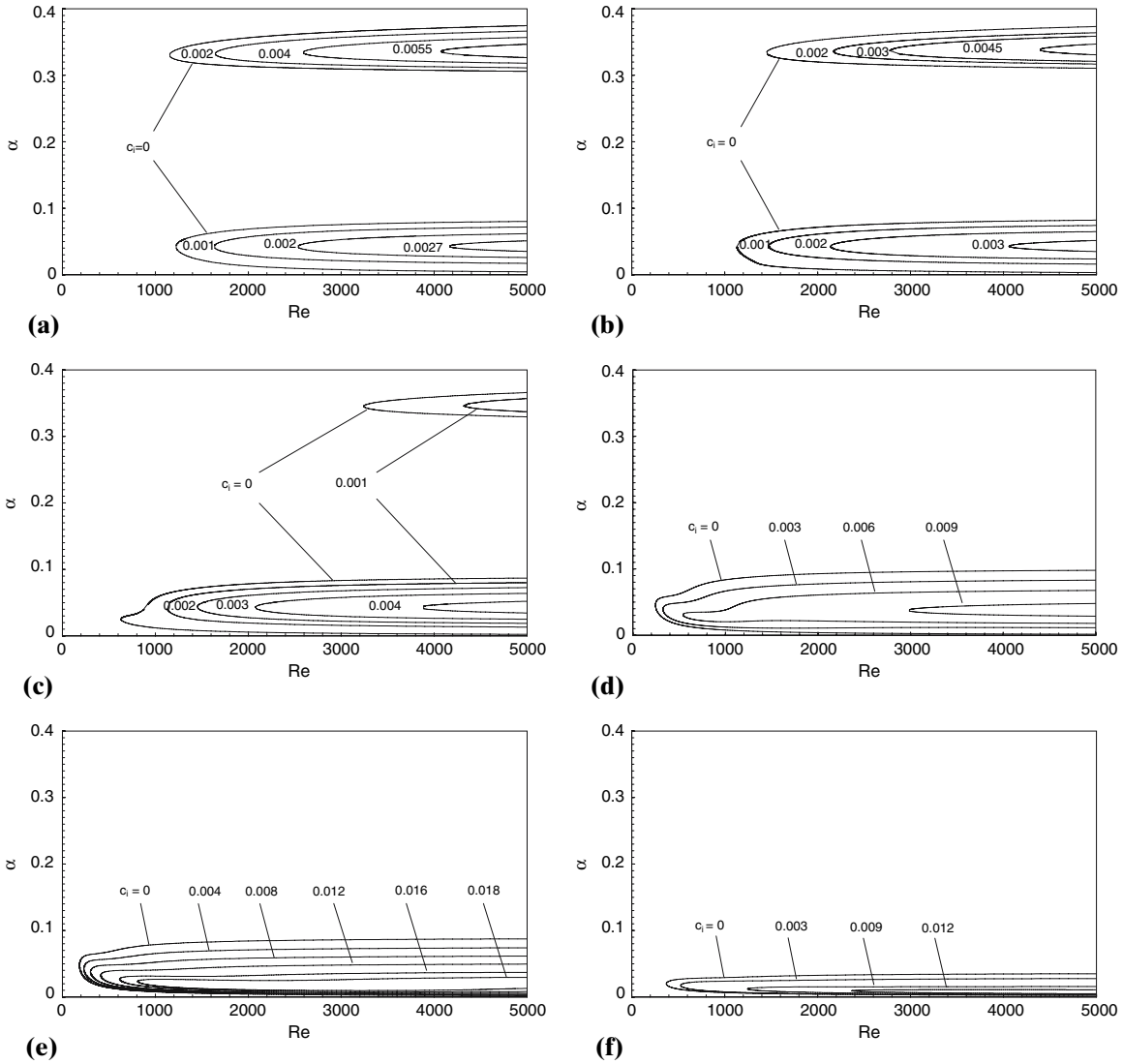


Fig. 6 Variation of the stability curves with wave angle for $M = 4$. **a** $\Psi = 0°$, **b** $\Psi = 10°$, **c** $\Psi = 20°$, **d** $\Psi = 40°$, **e** $\Psi = 60°$ and **f** $\Psi = 80°$

inclinations. Nevertheless, there is a significant stabilization for wave angles greater than 60°. From Fig. 6f we see that not only the range of unstable wave numbers shrink considerably but also the amplification factors decrease slightly.

Meanwhile in Fig. 7, the variation of the critical Reynolds numbers with the wave angle is illustrated for several Mach numbers. One observes that for Mach numbers up to unity, the most unstable waves (i.e., yielding the smallest critical Reynolds number) are two-dimensional. However, this changes rapidly once the Mach number is above one, and the most unstable wave direction shifts rapidly to 45° for $M = 2$, 55° for $M = 3$ and 60° for $M = 4$. For higher values of the Mach number, the most unstable wave direction remains close to 60°. From Fig. 7e, f, we also observe that three dimensionality has a very strong stabilizing effect on the second mode. These inferences are in agreement with the results outlined by Mack [2].

Figure 8 reveals a rather interesting phenomenon. It depicts the stability diagrams for the wave angles yielding the smallest critical Reynolds number for various Mach numbers. We observe that for $M \leq 1$ the stability diagrams show the characteristics of viscous instability, whereas for $M > 2$ they demonstrate inviscid instability characteristics. When $M > 2$, the most unstable wave direction remains almost constant at around $\Psi = 60°$. What is more interesting is that for $M > 4$, not only the critical Reynolds number remains constant but also the stability diagrams look extremely similar to each other with the unstable wave number ranges being

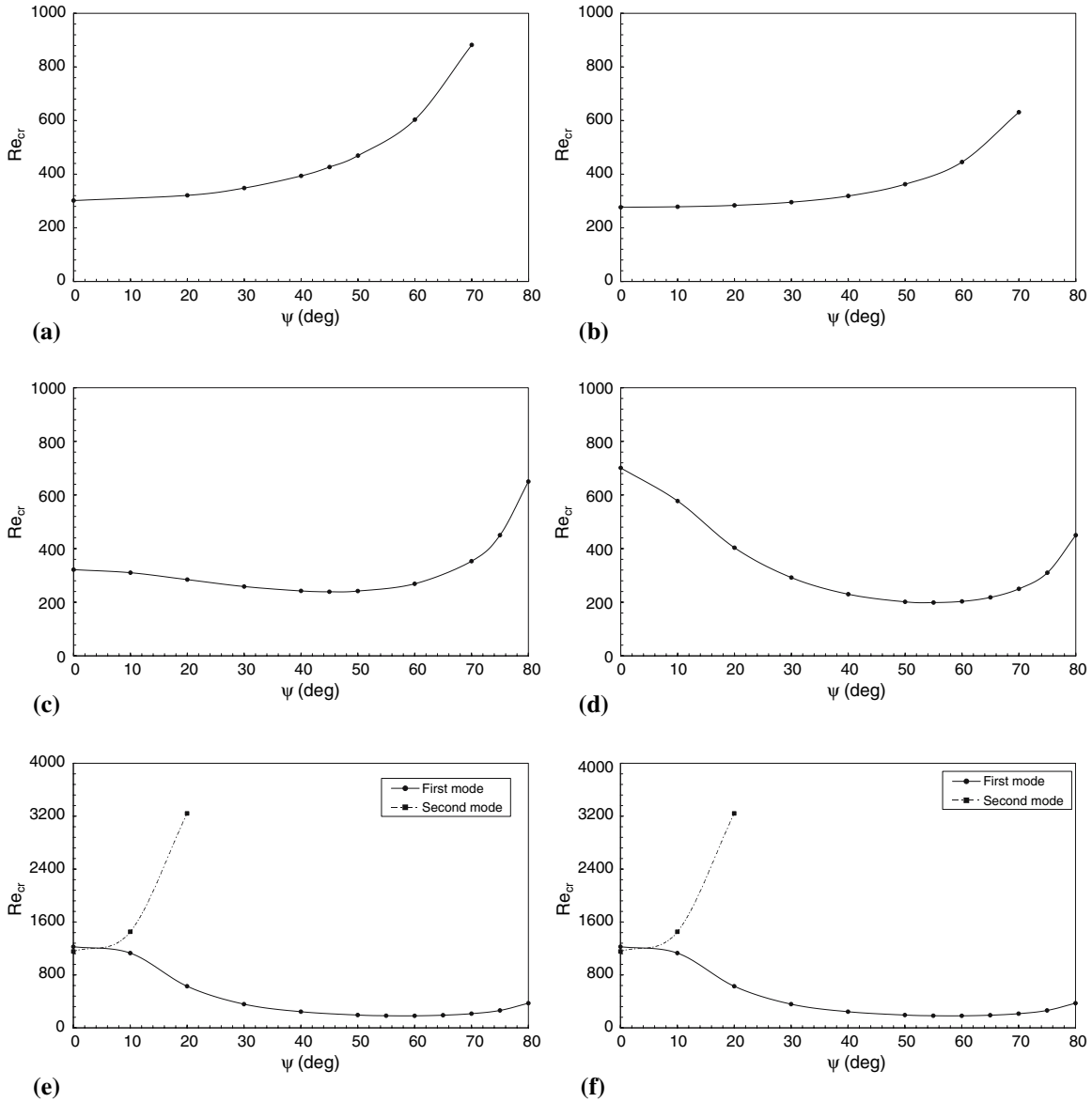


Fig. 7 Variation of the critical Reynolds numbers with wave angle. **a** $M = 0$, **b** $M = 1$, **c** $M = 2$, **d** $M = 3$, **e** $M = 4$ and **f** $M = 6$

confined to $0 < \alpha < 0.1$. Also, the amplification factors are almost identical with the highest amplification factor universally being around 0.02. These observations suggest that the stability characteristics become a weaker function of the Mach number when $M > 4$ for three-dimensional disturbances. This inference has not been reported or mentioned in the available literature to the authors' best knowledge. Yet, it may be related to the well-known *Mach number independence* principle in hypersonic flows [24,25].

5 Effect of reference temperature on stability characteristics

This section concentrates on the effects of the choice of the reference temperature on stability characteristics. Although dimensionless forms of the stability equations are solved in this study, the empirical formulas used for defining the temperature-dependent fluid properties require choosing a reference temperature and this has an effect on the results as demonstrated below.

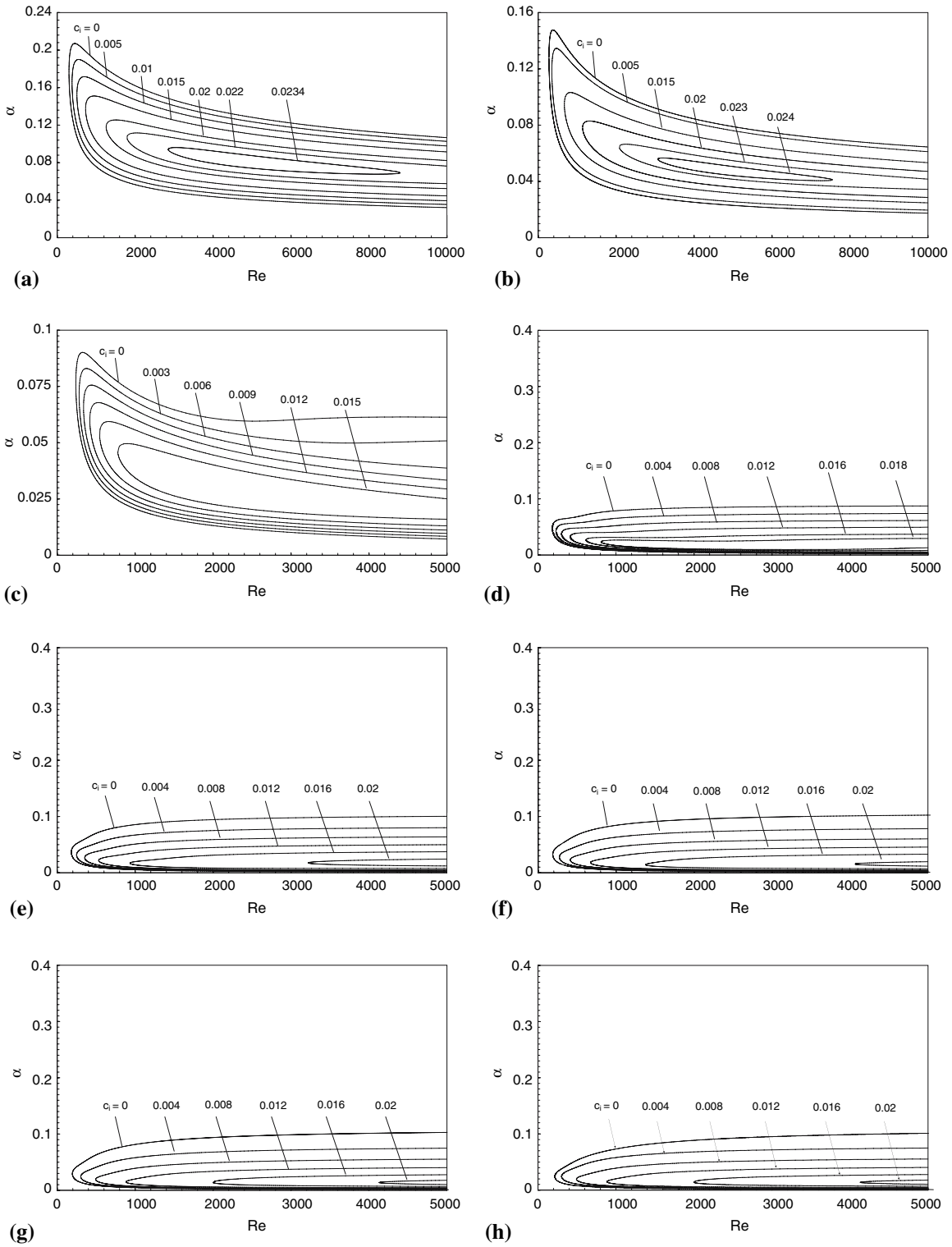


Fig. 8 Stability curves for the most unstable wave directions. **a** $M = 0, \Psi = 0°$, **b** $M = 1, \Psi = 0°$, **c** $M = 2, \Psi = 45°$, **d** $M = 4, \Psi = 60°$, **e** $M = 6, \Psi = 60°$, **f** $M = 7, \Psi = 60°$, **g** $M = 8, \Psi = 60°$ and **h** $M = 10, \Psi = 60°$

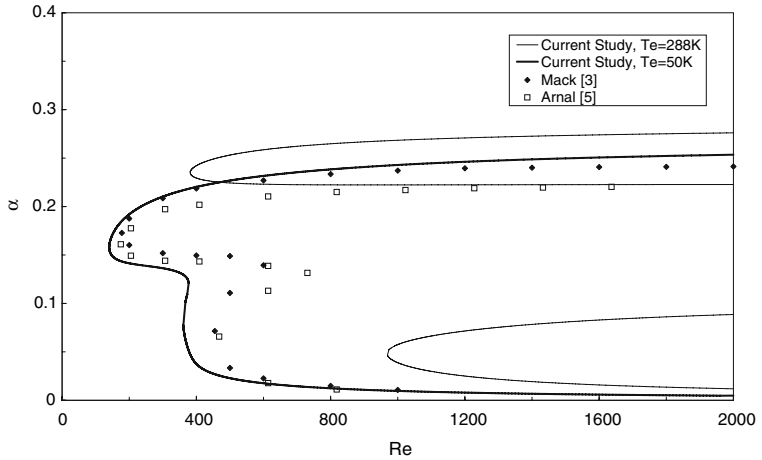


Fig. 9 Effect of reference temperature on stability characteristics and comparison with Mack [3] and Arnal [5] for $M = 4.8$ and $\Psi = 0°$

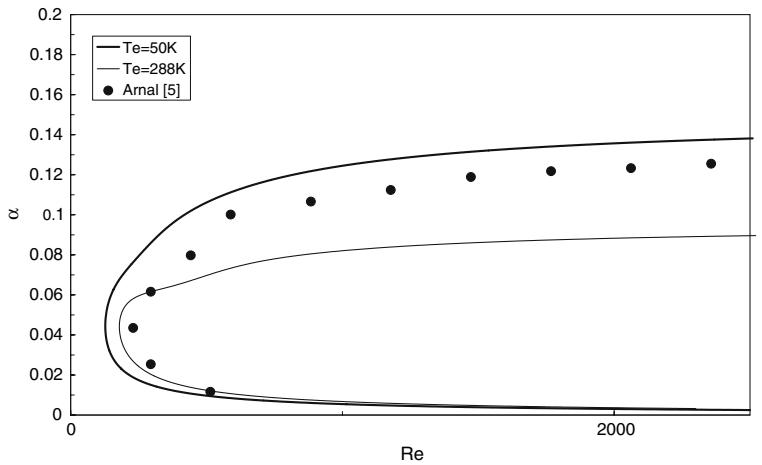


Fig. 10 Effect of reference temperature on stability characteristics and comparison with Arnal [5] for $M = 4.5$ and $\Psi = 60°$

Figure 9 shows how important this choice can be. Here, the neutral stability curves for $M = 4.8$ are compared for $T_e^* = 50\,\mathrm{K}$ and $T_e^* = 288\,\mathrm{K}$ for two-dimensional disturbances. In the case of $T_e^* = 288\,\mathrm{K}$, both the first and the second modes are present with two separate neutral stability curves. For the $T_e^* = 50\,\mathrm{K}$ case, we see a single neutral stability curve, meaning that the two modes have merged, a phenomenon that is observed at $M = 7$ for $T_e^* = 288\,\mathrm{K}$ (see Fig. 3). Results given by Mack [3] and Arnal [5] have also been included in the figure for comparison. On the one hand, we observe that the agreement of the results for $T_e^* = 50\,\mathrm{K}$ is acceptable, all three studies predicting similar critical Reynolds numbers and unstable wavenumber ranges. On the other hand, the results obtained for $T_e^* = 288\,\mathrm{K}$ are significantly different. This discrepancy can be attributed to the way variable fluid properties are treated and different formulations used. As mentioned above, Arnal has used spatial amplification formulation, while temporal formulation is used in this study. Although the neutral stability curves must be identical in both formulations, the solution methods are completely different, which may be a contributing factor to the discrepancy. Although it is unclear how the variable fluid properties are treated in Arnal's study, the empirical formulae used by Mack to represent the temperature dependence of the heat conduction coefficient is quite different from the one used here. Yet, one would still expect better agreement of the results of the current study and Mack's, as the formulation and the solution methods are similar. Furthermore, when one remembers the near-perfect agreement with the results of Masad et al., where there is less commonality both in the formulation and the solution method with the current study, it is rather unexpected that the current results and those of Mack do not agree better.

A similar comparison is performed for three-dimensional disturbances. Figure 10 illustrates the effect of reference temperature on the neutral stability curves for $M = 4.5$ and $\Psi = 60°$. Evidently, the effect of

reference temperature is less pronounced for oblique waves than it is for two-dimensional waves. Again, the results for $T_e^* = 50\,\mathrm{K}$ case is in better agreement with the results given in the literature. Obviously, the effect of reference temperature is more significant for high Mach numbers, for which temperature gradients are strong, i.e., effect of temperature field is more important. However, for three-dimensional disturbances, the effect is less obvious.

6 Conclusions

Stability characteristics of compressible flat-plate boundary layers are determined using the LST. The results confirm that as soon as there is relative supersonic flow, a second mode of instability (Mack mode) is observed in addition to the usual first mode, more prominently for two-dimensional disturbances.

The second mode is rapidly stabilized as wave inclination is increased and only the first mode is observed for high wave angles. The most unstable wave directions are typically around $\Psi = 60^\circ$ for moderate and high Mach numbers.

The reference temperature has proven to play an important role on the stability characteristics, especially for high Mach numbers. This parameter even determines whether or not the inviscid second mode is unstable at high Mach numbers.

Probably the most interesting and important result of this study is the behavior of the stability curves for $M > 4$ for oblique waves. The stability characteristics remain almost unaltered as the Mach number is increased beyond 4 up to 10, provided that the wave orientation does not change. To the authors' best knowledge, this is a novel result.

The data obtained are compared with numerical data in the literature yielding acceptable to good agreement depending on the case. The discrepancies are mainly attributed to different reference temperatures chosen by different researchers, use of different empirical formulae for temperature-dependent fluid properties, and use of different formulations or a combination of all.

As a result, the wide range of Mach numbers treated, detailed analysis of stability characteristics and encouraging agreement of the results with experimental and numerical data in the literature renders this study worthwhile.

References

1. Lees, L., Lin, C.C.: Investigations of the stability of the laminar boundary layer in a compressible fluid, NACA TN 1115 (1946)
2. Mack, L.M.: Linear stability theory and the problem of supersonic boundary-layer transition. AIAA J. **13**(3), 278–289 (1975)
3. Mack, L.M.: Boundary-layer linear stability theory. AGARD R 709 (1984)
4. Malik, M.R.: Prediction and control of transition in supersonic and hypersonic boundary layers. AIAA J. **27**(11), 1487–1493 (1989)
5. Arnal, D.: Boundary-layer transition: predictions based on linear theory. AGARD R 793 (1994)
6. Masad, J.A., Abid, R.: On transition in supersonic and hypersonic boundary-layers. Int. J. Eng. Sci. **33**(13), 1893–1919 (1995)
7. Malik, M.R., Anderson, E.C.: Real gas effects on hypersonic boundary-layer stability. Phys. Fluids A **3**(5), 803–821 (1991)
8. Malik, M.R.: Hypersonic flight transition data analysis using parabolized stability equations with chemistry effects. J. Spacecr. Rockets **40**(3), 332–344 (2003)
9. Laufer, J., Vrebalovich, T.: Stability and transition of a supersonic laminar boundary-layer on a flat-plate. J. Fluid Mech. **9**, 257–299 (1960)
10. Kendall, J.M.: Supersonic boundary-layer experiments. In: McCauley, W.D. (ed.) Proceedings of Boundary Layer Transition Study Group Meeting II, Aerospace Corp. (1967)
11. Kendall, J.M.: Wind tunnel experiments relating to supersonic and hypersonic boundary-layer transition. AIAA J. **13**, 290–299 (1975)
12. Coles, D.: Measurements of turbulent friction on a smooth flat-plate in supersonic flow. J. Aeronaut. Sci. **21**(7), 433–448 (1954)
13. Deem, R.E., Murphy, J.S.: Flat-plate boundary-layer transition at hypersonic speeds. AIAA Paper 65–128 (1965)
14. Laufer, J., Marte, J.E.: Results and a critical discussion of transition-Reynolds number measurements on insulated cones and flat-plates in supersonic wind tunnels. Jet Propulsion Lab, Pasedena, CA, Rept. 20-96 (1955)
15. Chen, F.-J., Malik, M.R., Beckwith, I.E.: Boundary-layer transition on a cone and flat-plate at Mach 3.5. AIAA J. **27**(6), 687–693 (1989)
16. Schlichting, H.: Boundary-layer theory, vol. 7. McGraw-Hill, Inc., New York (1979)
17. The Mathworks, Inc., MATLAB: the language of technical computing (2004)
18. Mathews, J.H.: Numerical methods. Prentice-Hall, London (1987)
19. Mack, L.M.: A numerical study of the temporal eigenvalue spectrum of the Blasius boundary-layer. J. Fluid Mech. **73**(3), 497–520 (1976)

20. Press, W.H., Teukolsky, S.A., Vetterling, W.T., Flannery, B.P.: Numerical recipes in Fortran 77. Cambridge University Press, Cambridge (1992)
21. Pruett, C.D., Streett, C.L.: A spectral collocation method for compressible, non-similar boundary-layers. Int. J. Numer. Methods Fluids **13**, 713–737 (1991)
22. Obremski, H.J., Morkovin, M.V., Landahl, M.: A portfolio of stability characreristics of incompressible boundary-layers. AGARDograph 136 (1969)
23. Özgen, S.: Effect of Heat Transfer on stability and transition characteristics of boundary-layers. Int. J. Heat Mass Transf. **47**, 4697–4712 (2004)
24. Hayes, W.D., Probstein, R.F.: Hypersonic flow theory. Academic, New York (1959)
25. Anderson, J.D.: Modern compressible flow. McGraw-Hill, New York (1990)
26. Laufer, J.: Some statistical properties of the pressure field radiated by a turbulent boundary layer. Phys. Fluids **7**(8), 1191–1197 (1964)
27. Schubauer, G.B., Skramstad, H.K.: Laminar boundary-layer oscillations and transition on a flat-plate, NACA Report 909 (1946)